Comparisons of Properties in a Squall Line Between Observations and Bin Microphysics Simulations

Xue, L.[1], Lebo, Z.[2], Fan, J.[3], Bansemer, A.[1], Geresdi, I.[4], North, K.[5], Morrison, H.[1], Rasmussen, R.[1], Thompson, G.[1], Grabowski, W.[1], Kollias, P.[5], and Heymsfield, A.[1]

1. NCAR, 2. NOAA, 3. PNNL, 4. University of Pecs, 5. McGill University

Introduction

A squall line event on May 20, 2011 has been measured in detail by several remote sensing platforms and airborne instruments during the Midlatitude Continental Convective Clouds Experiment (MC3E). This well documented case is simulated by three different state-of-the-art bin (spectral) microphysics schemes coupled into WRF V3.4.1 to investigate the dynamical and microphysical properties of the squall line through model and observation comparisons. Brief comparisons between model results, C-SAPR radar reflectivity and in-situ aircraft observations are presented. In-depth analyses in the near future will quantify differences in organized deep convection among bin model simulations, with implications for their use as benchmarks in testing and improving bulk microphysics schemes.

Model Description and Case Setup

The three bin microphysics schemes used in this work are all mixed-phase schemes applying mass doubling bins. Scheme 1 was developed based on the mixed-phase scheme originated from Tel Aviv University (1-5). Scheme 2 was developed based on the warm-phase version of the same Tel Aviv scheme (6-7). Scheme 3 was developed in the Hebrew University, known as the SBM scheme (8-10). Both schemes 1 and 2 use the method of moments (11) while scheme 3 applies flux method (12) to ensure the conversation of number and mass over all bins. The detail of these schemes can be found in the references.
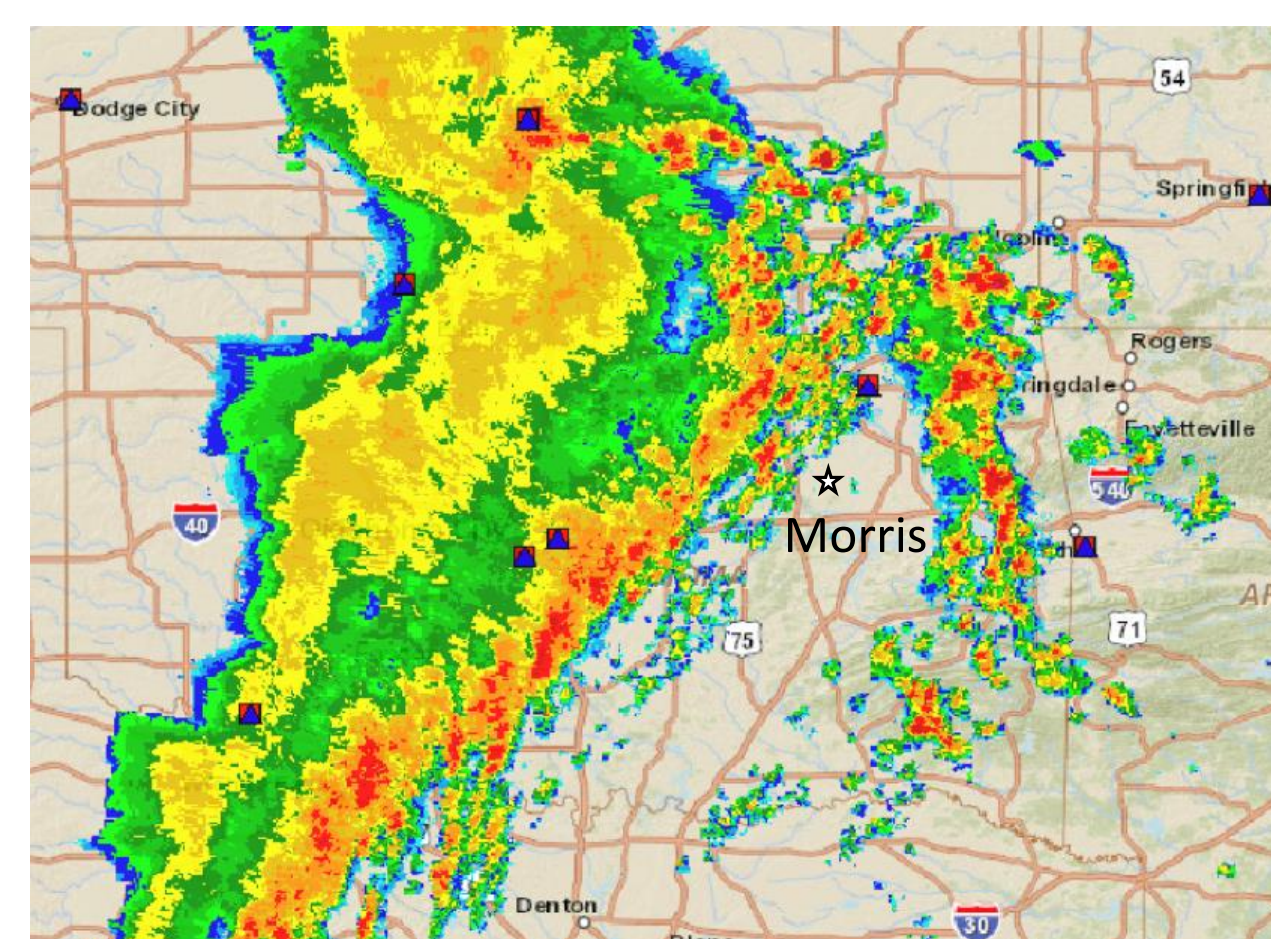

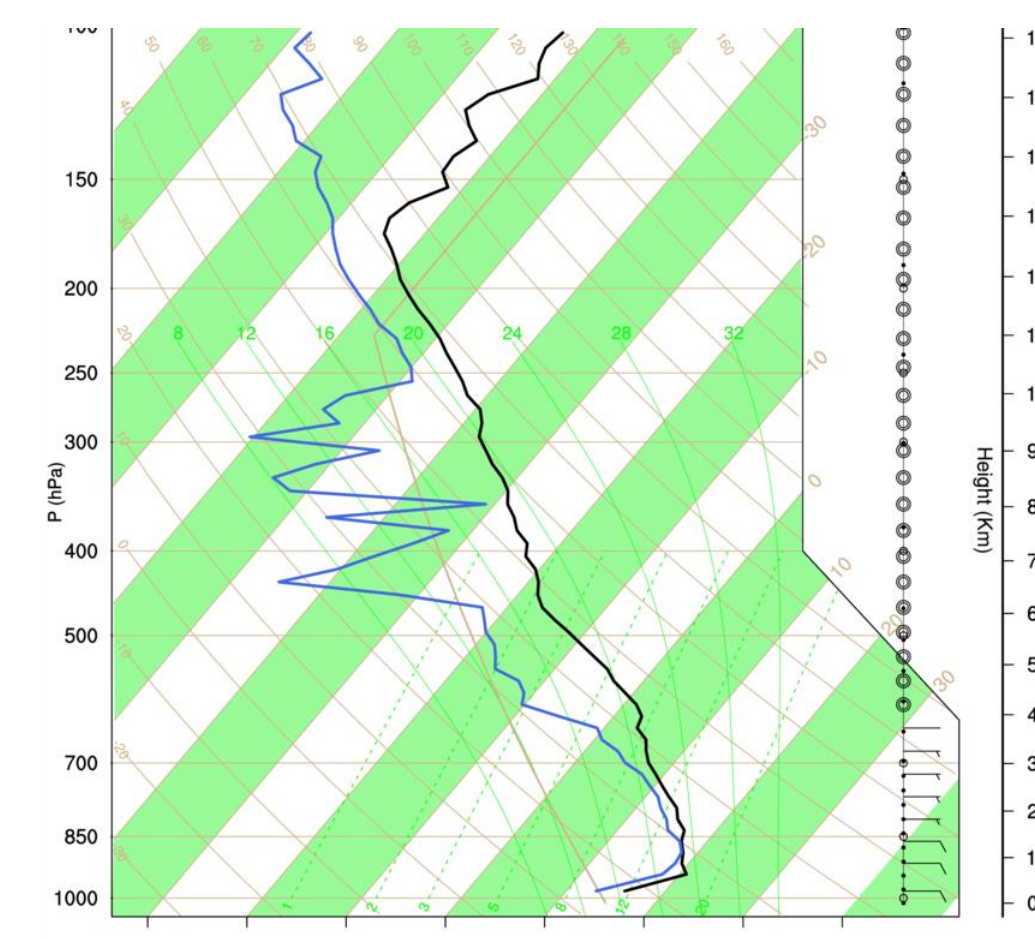Figure 1. Sounding location relative to squall line at 1200 UTC.

Figure 2. Sounding for the idealized WRF simulations.

On May 20, 2011, rawinsondes were launched at high frequency to capture the storm environmental structure. We found the sounding at 1200 UTC from site Morris is of particularly useful due to its good representation of pre-convection conditions (Fig. 1). The observed thermodynamic profile shows a moist low level air and a unstable layer between 4 and 6 km. The CAPE is 2200 J from 900 m up. This observed profile and adjusted wind field were used to drive the WRF simulations.

We simulate this case for 6 hours in a 3D setup. There are 612 by 122 grids in horizontal with a grid spacing of 1 km. Vertically, 100 levels cover 25 km with semi-uniform grid spacing. The opened boundary condition is applied in x direction while the periodic condition is used in y direction. The dynamic time step is set to 3 seconds. Radiation, PBL scheme and surface physics are all turned off. A Rayleigh damping layer is applied to the top 5 km of the domain to reduce the reflection of the vertical waves. The convection is initiated in the center by a mass convergence in x direction reducing with time during the first hour of the simulation.

Model Radar (C-SAPR) Comparison

Figure 3 shows examples of the y-averaged radar reflectivity at the end of the simulations from two schemes. In general, both schemes generated squall lines but also simulated very different structures.
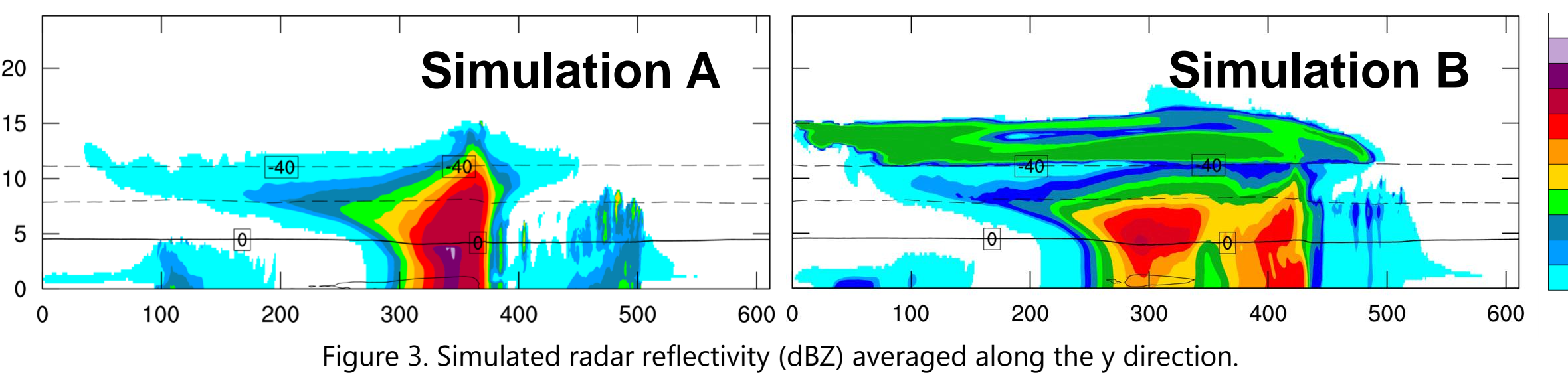

Figure 3. Simulated radar reflectivity (dBZ) averaged along the y direction.

C-SAPR recorded detailed reflectivity information of this event within the "inner SGP grid" region (about 100 km by 100 km) from 0500 to 1230 UTC on May 20. Examples of plan views of the gridded reflectivity at 1019 UTC at different levels are illustrated in the top panels of Figure. 4. The model simulated counterparts are shown below the observations. Since C-SAPR has a wave length of about 5 cm at which Rayleigh scattering is still valid for most of the hydrometeors, therefore we calculate the model reflectivity explicitly using all bins under the assumption of Rayleigh scattering.
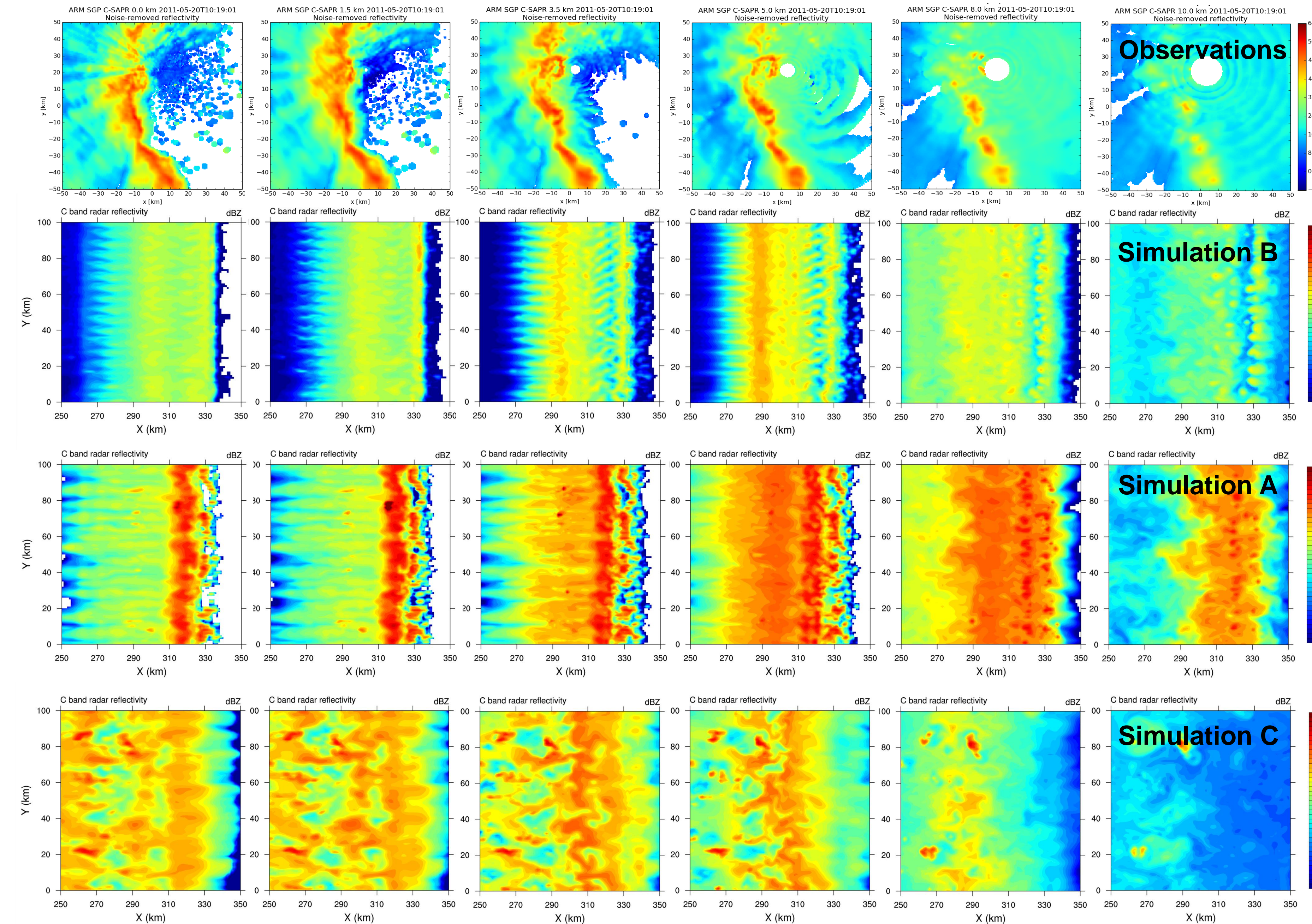

Figure 4. Plan views of C-band radar reflectivity at 0, 1.5, 3.5, 5.0, 8.0 and 10.0 km from C-SAPR at 1019 UTC (top panels) and model counterparts from three schemes at different times (lower panels).

The bin schemes are able to simulate a well-defined convective linear structure and trailing stratiform structure in similar dBZ magnitude through out the storm depth compared to C-SAPR observations. However, the simulated squall lines are relatively wider and deeper than the observed one. Similar to Figure 3, the inter-model variability is also very high in Figure 4.

The contour frequency by altitude diagrams (CFADs) of the C-SAPR observed reflectivity within the "inner SGP grid" and model simulated counterparts (within 100 km by 100 km area) are plotted in Figure 5. The model CFADs are from three schemes at different times. Model generally simulated a higher reflectivity field. The observed high reflectivity below melting layer is captured by the model (see the right panels for details). In general, the model radar comparison showed that bin schemes are capable of getting the squall line structure right.
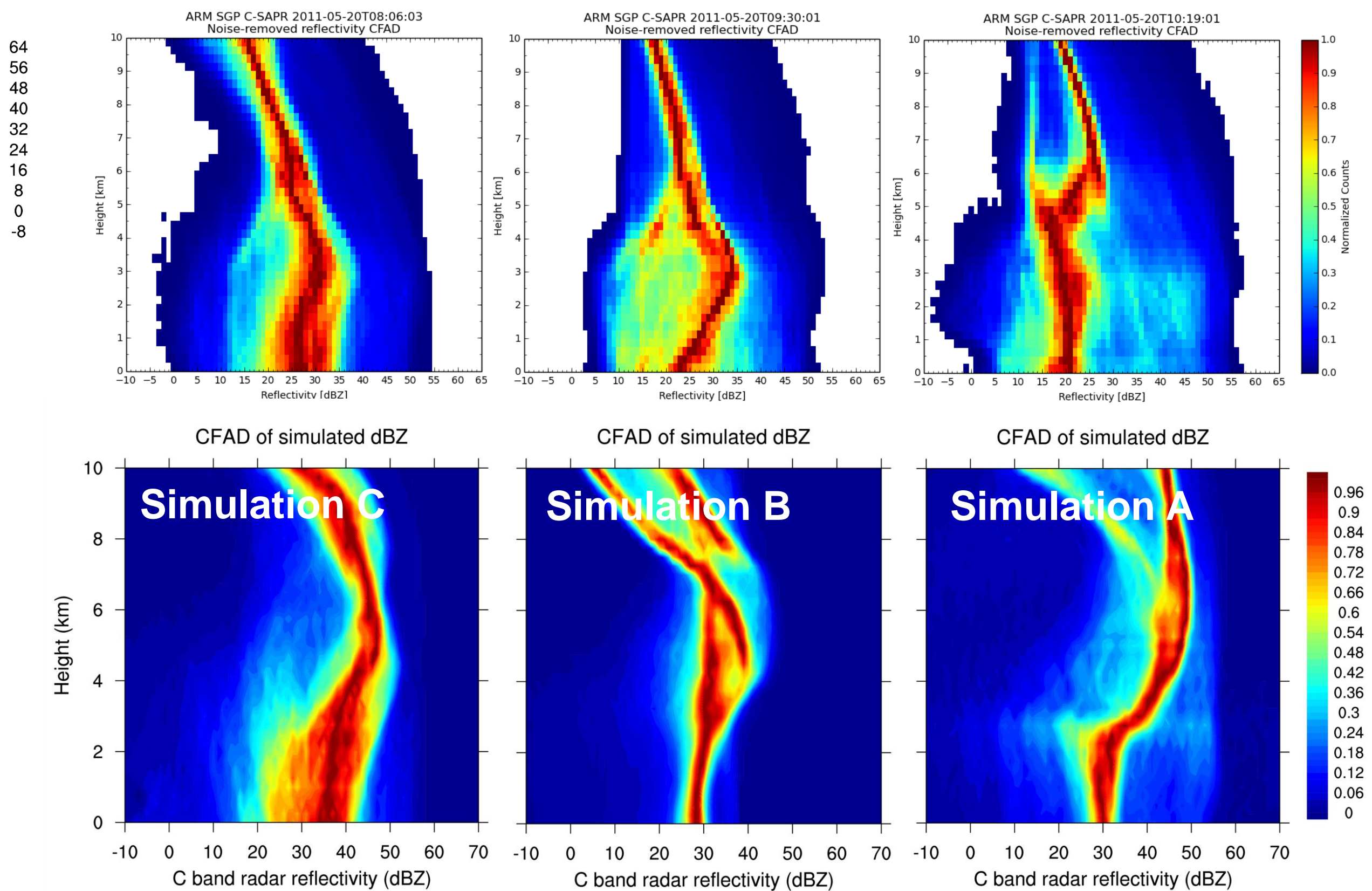

Figure 5. CFADs of observed C-SAPR reflectivity and model simulated reflectivity.

Model In-situ Observations Comparison

The microphysics research aircraft, UND CITATION, conducted many penetrations of the trailing stratiform of the squall line to map out microphysical pathways associated with particle growth and melting (Figure 6). Both observed and simulated particle size distributions (> 250 um) show that small ice particles grow downward from cold region to melting layer. When such particles fall through the melting layer, they become drops in smaller sizes (Figure 7).
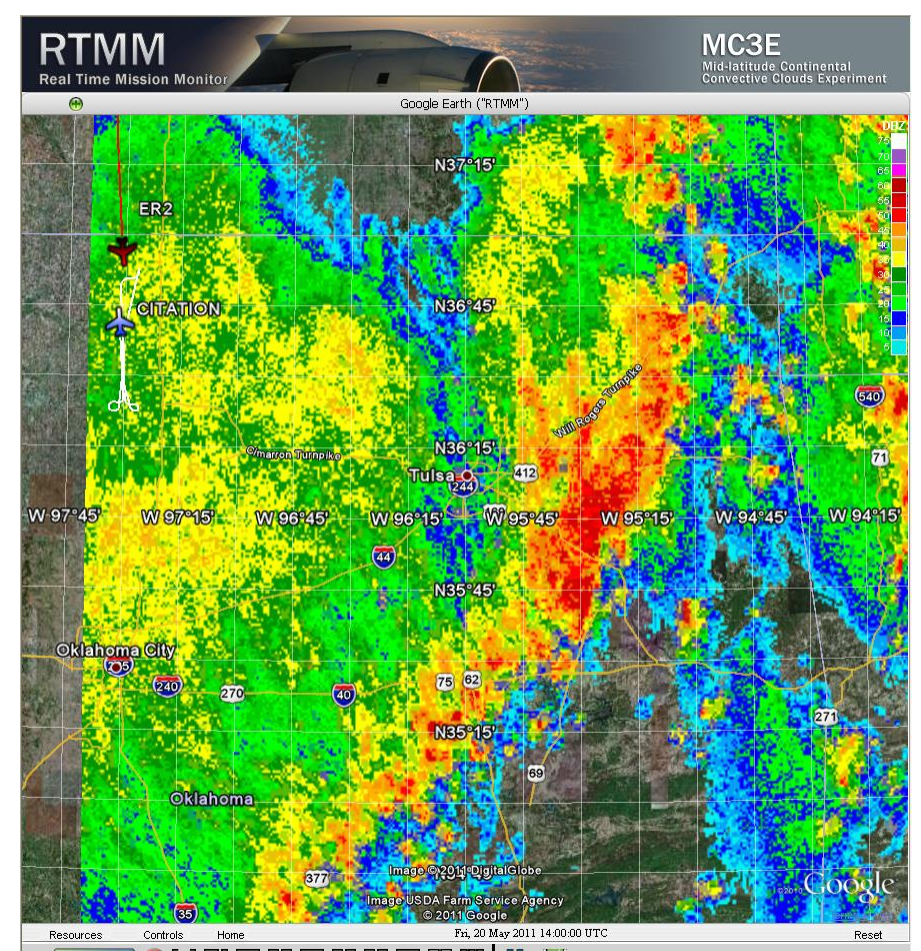

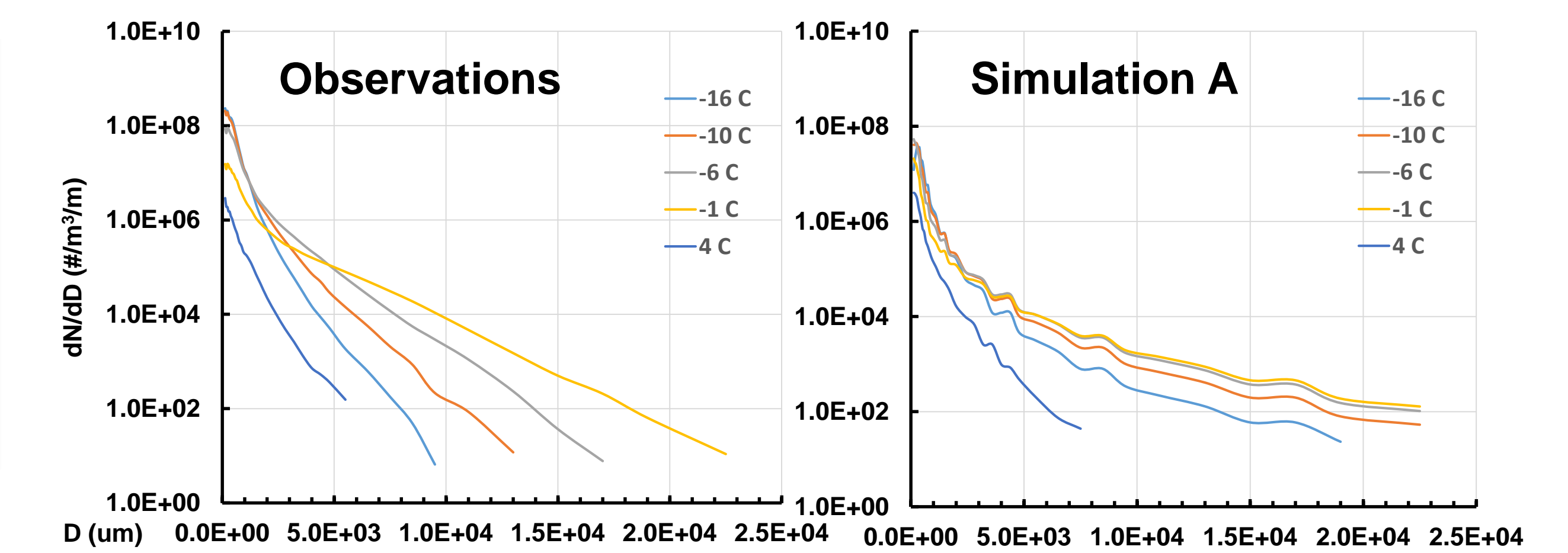Figure 6. Schematic of CITATION flight patterns.

Figure 7. Observed and simulated ensemble averaged size distributions at different levels of the stratiform region.

Summary

The model observations comparisons show that the bin schemes can reproduce squall line structure and particle size evolution. There is a large spread of results simulated by different bin schemes.

References: 1. Reisin et al., JAS, 1996. 2. Geresdi, AR, 1998. 3. Rasmussen et al., JAS, 2002. 4. Xue et al., JAS, 2012. 5. Geresdi et al., AR, 2014. 6. Lebo and Seinfeld, ACP, 2011. 7. Feingold et al., JAS, 1988. 8. Khain et al., JAS, 2004. 9. Khain et al., JGR, 2009. 10. Fan et al., JGR, 2012. 11. Tzivion et al., JAS, 1987. 12. Bott, JAS, 2000.